Advanced Powder Technology xxx (xxxx) xxx

Contents lists available at ScienceDirect

Advanced Powder Technology

journal homepage: www.elsevier.com/locate/apt

Original Research Paper

A novel, eco-friendly and green synthesis of PPAC-ZnO and PPAC-nZVI nanocomposite using pomegranate peel: Cephalexin adsorption experiments, mechanisms, isotherms and kinetics

Yousef Rashtbari [a,b], Sadegh Hazrati [a], Ali Azari [c], Shirin Afshin [a,b], Mehdi Fazlzadeh [a,d,e,*], Mehdi Vosoughi [a,e,*]

[a] Department of Environmental Health Engineering, School of Health, Ardabil University of Medical Sciences, Ardabil, Iran
[b] Students Research Committee, Faculty of Health, Ardabil University of Medical Sciences, Ardabil, Iran
[c] Department of Environmental Health Engineering, School of Public Health, Kashan University of Medical Sciences, Kashan, Iran
[d] Department of Environmental Health Engineering, School of Public Health, Tehran University of Medical Sciences, Tehran, Iran
[e] Social Determinants of Health Research Center, School of Health, Ardabil University of Medical Sciences, Ardabil, Iran

ARTICLE INFO

Article history:
Received 17 July 2019
Received in revised form 7 November 2019
Accepted 3 February 2020
Available online xxxx

Keywords:
Cephalexin
Adsorption
Green synthesis
Activated carbon
nZVI

ABSTRACT

In the present work, powdered activated carbon coated by nanoparticles ZnO and nZVI was derived from pomegranate peel extracts and finally applied for removal of cephalexin (CEX (from aqueous solutions. This experimental research was conducted discontinuously. The effects of pH of solution, reaction time, PPAC-nZVI and PPAC-ZnO composites dose, and initial concentration of cephalexin and composite recovery on process efficiency were investigated. The removal efficiency in optimal conditions for cephalexin with PPAC-nZVI and PPAC-ZnO (CEX = 50 mg L^{-1}, composite dose = 1.25 g L^{-1}, reaction time = 45 min and pH = 5) was obtained 96.06% and 94.17%, respectively. The results of the study of isotherm and absorption kinetics for both composites showed that the absorption process follows Langmuir isotherm and pseudo second-order kinetics. The present study showed that the composites could be used as an effective and bio-friendly absorbent to remove cephalexin from aqueous solutions.

1. Introduction

In recent years, environmental problems involving the pollution of water resources with antibiotic compounds have become a serious problem [1,2]. Antibiotics are categorized as emerging pollutants and generally produced by the pharmaceutical, agriculture, and biomanufacturing industries and discharged into the environment. About 30–90% of the given dose of antibiotics can remain as un-metabolized form in the human or animal bodies [3,4]. This amounts of antibiotics are excreted through urine and feces into the receiving water as active compounds [5,6]. In other side, conventional wastewater treatment processes can only remove a range of 60–90% of some antibiotics that result in increasing bacterial resistance in the environment and lead to disease if transmitted to human's body [7,8]. Cephalexin (CEX) is the first-generation of cephalosporin that widely used for treating a variety of infections of body system such as ear, skin, and soft tissue, skeletal, urinary and respiratory tract [9]. Due to the low degradability of the antibiotics in the environments, high concentrations of antibiotics may sometimes occur in wastewater treatment plants and also in drinking water [10,11]. Long term exposure to antibiotics can cause health problems in human and pose serious threats to the ecosystem [12,13]. Accumulated concentrations of cephalexin in drinking water can result in mutagenic and carcinogenic impacts in human body [14]. Hereupon is very pivotal and imperative for the development of effective and economical techniques for the uptake of huge flux of selected antibiotics. Several methods such as membrane separation [15], biological technique [16], sonochemical process [17], electro-Fenton oxidation [18], reverse osmosis [19] and adsorption [14] have been employed for the removal of CEX from aqueous solution. Whereas, most of the above mentioned methods are not suitable due to low efficiency, require to pre-treatment, high operational cost, hazardous byproducts, high energy requirement [20,21].

Among the mentioned methods, adsorption process is used as a sludge-free, simple, effective, promising and available techniques

* Corresponding authors at: Department of Environmental Health Engineering, School of Health, Ardabil University of Medical Sciences, Ardabil, Iran.
E-mail address: m.fazlzadeh@gmail.com (M. Fazlzadeh).

https://doi.org/10.1016/j.apt.2020.02.001
0921-8831/

for the treatment of many pollutants in water and wastewater [22]. Despite all the positive features and advantages of nanomaterials i.e. ZnO and nZVI as ideal adsorbent, their separation after adsorption process by filtration and centrifugation is difficult and still remain as challenge. According to the literatures, this problem can be countered by using the support such materials as oxides, polymers, fibers and active carbon in the adsorbent structure. Moreover, the use of the stabilized nanomaterials in large-scale is more cost-effective and practical for the fact that there is no need for separating the adsorbent upon the termination of the process [23,24]. Therefore, researches have focused on developing the Active Carbon (AC) as support due to its high availability, low cost, large surface area, and reusability, chemical properties of its surface and large volume of its pores [25–27]. In previous literatures, many researchers have pointed out that the adsorbent based AC support are easily separated from the reaction media, regenerated and reused, which generally reduce the cost and energy [28,29].

Until this part of the research, the role of ZnO, nZVI nanoparticles (NPs) and AC in CEX adsorption was expressed, but there is still an important issue that has not been addressed. In the last decades, NPs have been widely used in water and wastewater treatment process (1). In most cases, NPs synthesized by chemical processes including hazardous chemicals, reducing agents, and capping agents under controlled conditions. They are expensive and contact with them (in the case of discharge into the environment without treatment and access to the necessary standard) can have side effects for humans, beings and the environment. Recently, researchers have reported green synthesis of NPs according to the plant-based products is an appropriate and alternative method for chemical synthesis (2–10). Plant-based green-synthesized NPs are as active as their chemically synthesized counterparts; furthermore, they can be rapidly synthesized and are environmentally friendly. The Minerals, organic acids, phenolics, proteins, and enzymes that are in the structure of plants (e.g., leaf and fruit) including the many reducing, oxidizing, capping, and stabilizing components, which enhance the synthesis of NPs (13).

Pomegranate is an inexpensive product that has been extensively cultivated and used in Iran. This fruit is also used in culinary, pharmaceutical and cosmetic industries in the world. The pomegranate peel makes up more than 50% of the fruit weights, which is discarded as garbage. Previous studies suggest that minerals (e.g., potassium), vitamins, phenolics, flavonoids, and antioxidants are the part of nutrient content which can be extracted from pomegranate peel and used to synthesis of nanoparticles [30,31].

Based on the information mentioned above, in summary, this study focused on the (i) synthesis of ZnO and nZVI nanoparticles using pomegranate peel extract (PPE) and their characterizing by FESEM, FTIR, EDAX and BET analysis (ii) Preparation of activated carbon derived from pomegranate peel (PP) as support for ZnO and nZVI NPs loading and its characterizing by FESEM, FTIR, EDAX and BET analysis (iii) Determining the impact of effective parameters i.e pH, adsorbent dose, initial concentration and contact time on CEX removal efficiency [32] Investigating the adsorption equilibrium and kinetic to examine adsorption behavior of CEX onto PPAC-ZnO and PPAC-nZVI nanocomposite; and determining the adsorption mechanism of CEX onto the PPAC-ZnO and PPAC-nZVI nanocomposite

2. Materials and methods

2.1. Materials

The chemicals were prepared from Merck. Co (Germany): ferric chloride hexahydrate ($Fecl_3{\cdot}6H_2O$, 97%), ferrous chloride Tetrahydrate ($Fecl_2{\cdot}4H_2O$, 98%), methanol (CH_3OH, ACS grade), sodium hydroxide (NaOH, 93%), and hydrochloric acid (HCl, 35–37%). Cephalexin ($C_{16}H_{17}N_3O_4S$; MW = 347.39 g mol^{-1}, 97%) was purchased from Sina Daru, Ltd. (Tehran, Iran). The reagents were used as received without further purification. All solutions were prepared with double distilled water. CEX stock solution (1000 mg L^{-1}) was obtained by dissolving a specific amount of sodium salt of cephalexin in DI water and diluted in desired concentrations.

2.2. Preparation the pomegranate peels based activated carbon (PPAC)

Pomegranate Peels (PP) were collected from Ardabil province [33], washed several times with DI water to remove any dust and impurities and then dried in an oven at 100 °C for 2 h. PPs was sieved through a 60-mesh screen and then soaked in phosphoric acid (85 wt% H_3PO_4) with a ratio of 1:1 (w/w) for 48 h. Afterward, the dried materials were placed in a cylindrical steel reactor in furnace (5 °C/min) at 800 °C for 2 h. After cooling, the remaining black materials (pomegranate peel active carbon, PPAC) were rinsed several times with DI water to reach a pH = 7. Finally, PPAC was dried in an oven at 110 °C for 2 h and finally stored in a dry place for further use [34].

2.3. Green synthesis of nZVI and ZnO from pomegranate peel extract

Pomegranate peel was used to synthesize of nZVI and ZnO NPs. The extract of pomegranate was prepared by boiling of 60 g L^{-1} peel at 80 °C for 1 h and residual peels after precipitation were filtered by a vacuum pump. Then, $ZnCl_2$ solution (0.2 M) mixed with pomegranate peel extract (PPE) in the ratio of 1:2. After that, mixture was homogenized on ultrasonic bath (35 kHz) for 60 min. In the next step, a dark yellow colored precipitate was appeared when the pH of the solution was adjusted at 9 by adding diluted NaOH. The formed precipitate which show the formation of ZnO NPs. washed several times with ethanol and then rinsed with double distilled water, dried at 50 °C for 12 h. After drying the nanoparticles, it was transferred into a furnace with a temperature of 400 °C and remained at this temperature for 2 h. After cooling the furnace, the nanoparticles were collected and placed in nitrogen gas to avoid oxidation.

Also for synthesis of nZVI, a 0.1 M $FeCl_2{\cdot}4H_2O$ solution was prepared from $FeCl_2{\cdot}4H_2O$ into of deionized water. 0.1 M $FeCl_2{\cdot}4H_2O$ solution was then added into pomegranate peel extracts in the ratio 2:3. Afterward, the mixture was transferred into an ultrasonic bath and allowed to stay for 60 min. The pH value was adjusted to 6 by adding 1 M HCl. At this time, a black colored precipitate appeared which indicates the formation of pomegranate peel zero valent iron nanoparticles [35–39]. The formed NPs were separated by evaporation on a hot plate surface and collected by washing three times with deionized water and placed in nitrogen gas to prevent oxidation. The synthesized NPs were ground and stored for further use.

2.4. Coating ZnO and nZVI NPs on activated carbon (PPAC -ZnO and PPAC – nZVI)

After PPAC preparation and nZVI and ZnO synthesis, 0.05 g ZnO and nZVI were separately dissolved in 200 mL distilled water and agitated for 15 min to obtain equal distribution. In the next step, 5 g of PPAC was added to per suspension and agitated at 500 rpm for 10 h at room temperature (25 °C) to complete the coating process. Then the PPAC-ZnO and PPAC-nZVI was filtered and washed with double distilled water and placed in oven in 95 °C for 10 h to be completely dried [40].

Please cite this article as: Y. Rashtbari, S. Hazrati, A. Azari et al., A novel, eco-friendly and green synthesis of PPAC-ZnO and PPAC-nZVI nanocomposite using pomegranate peel: Cephalexin adsorption experiments, mechanisms, isotherms and kinetics, Advanced Powder Technology, https://doi.org/10.1016/j.apt.2020.02.001

2.5. Adsorbents characterization

The samples characteristic including surface area, pore volume and pore size were determined by N_2 adsorption at 77 K using a Micromeritics (Australia) Tristar 3000 analyzer coupled. Scanning electron microscopy (FE-SEM/EDX model Mira 3-XMU) was used for observed the morphological features of PPAC-ZnO and PPAC- nZVI. The instrument is combined with an EDX analyzer. The crystallographic structure of samples was studied by X-ray diffraction (XRD) at 25 °C by a Philips X-ray generator model with a PW 3700/30 control X-ray diffraction system (Quanta chrome, NOVA2000, USA), using Cu Ka radiation in the range of $2\theta = 20–80°$. The functional groups of the synthesized adsorbents were determined by fourier transform infrared spectroscopy (FTIR, FTS-165, BIO-RAD, USA). The samples were incorporated in KBr pellets and the spectra were obtained in the range of 400–4000 cm^{-1}.

2.6. Experiments procedure

2.6.1. Determination of point of zero charge (pH_{pzc})

The determination of pH_{pzc} of the samples was carried out as follows: initial pH a value of 50 mL of 0.1 M NaCl was applied as an electrolyte; the pH was adjusted in range of 2–12 by adding 0.1 M NaOH and/or HCl. Then, 0.1 g of sample added into each solution and has been shaken for 24 h under agitation at room temperature. After mixing, the adsorbent was filtered and the final pH of the solution (pH_f) was also determined. At the final step, the value of pH_{pzc} of adsorbent was found from the intersection of the curve of the initial pH and the final pH [41].

2.6.2. Adsorption study

The experiments study was performed in batch procedure and laboratory scale in 250 mL Erlenmeyer flask containing 100 mL of CEX solution with initial concentration range of 10–100 mg L^{-1}. The effect of effective parameters, including pH (3, 5, 7, 9 and 11), adsorbent dosage (0.1, 0.25, 0.5, 0.75, 1, 1.25, 1.5 and 2 g L^{-1}) and contact time (5, 15, 30, 45, 60, 75, 90 and 120 min) on removal efficiency were studied at room temperature. The solution pH was adjusted by 0.1 M NaOH or H_2SO_4 for each experiment. In the following, Pre-determined amount of absorbent was added to each Erlenmeyer flasks and kept in an incubator at room temperature until predetermined contact time (at 250 rpm). After predetermined contact times, the samples were centrifuged and filtered using a whatman paper (0.2 μm) and the residual concentration of CEX was determined by an HPLC-UV, equipped with a reverse phase column (C18 column, with an annulus of 4.6 mm and a length of 150 mm) and methanol carrier phase (30 to 70%) at the detection wavelength of 263 nm [42].

All experiments were performed in duplicate and average values were reported for ensuring the reliability of results. The CEX removal efficiency (R) and the equilibrium adsorption capacity (q_e) values were determined using Eq. (1) and, Eq. (2), respectively [33,43]:

$$R(\%) = \left(\frac{(C_o - Ce)}{C_o}\right) \times 100 \quad (1)$$

$$q_e(mg\ g^{-1}) = \frac{[(C_o - Ce) \times V]}{m} \quad (2)$$

where, C_0 (mg L^{-1}) and C_e (mg L^{-1}) are the initial and residual concentration of the CEX, respectively. V (L) is the CEX solution volume and M (g) is the weight of applied adsorbents.

2.7. Kinetic and isotherm modeling

In this study, the kinetics of CEX adsorption onto PPAC-ZnO and PPAC-nZVI were analyzed by using Pseudo-first order, Pseudo-second order, Elovich and Weber-Morris Intraparticle diffusion models. Moreover, the experimental equilibrium adsorption data were analyzed by Freundlich, Langmuir, Redlich-Peterson, and Temkin isotherm models (Table S1) [44–46]. The general forms of all kinetic and isotherm models (except the Weber –Morris Intraparticle kinetic model) were nonlinearly fitted to the experimental adsorption data using OriginLab Pro (2018) software.

The adsorption isotherms were studied using initial concentration of CEX range of 10–100 mg L^{-1} at the optimum conditions. The kinetics models were studied also over pre-determined time intervals with at optimum conditions at 70 min.

The fitting of kinetic and isotherm models was evaluated by the coefficient of determination (R^2) and the residual root-mean squared error (RMSE). R^2 and RMSE were calculated as follow [47,48]:

$$R^2 = 1 - \frac{\sum_{n=1}^{n}(q_{exp} - q_{cal})^2}{\sum_{n=1}^{n}(q_{cal} - \bar{q}_{cal})^2} \quad (3)$$

$$RMSE = \sqrt{\frac{1}{n-1}\sum_{n=1}^{n}(q_{exp} - q_{cal})^2} \quad (4)$$

where q_{cal} (mg g^{-1}) and qexp (mg g^{-1}) are the calculated- and experimental CEX adsorption capacities, respectively, and time t (kinetic) and at equilibrium (isotherm), while n is the number of data points. Higher R^2 (closer to 1) and lower RMSE (closer to 0) values indicate more accurate fitting of the models.

3. Results and discussion

3.1. Characterization of synthesized adsorbent

3.1.1. FESEM analysis

The surface morphology of PPAC, PPAC-ZnO and PPAC- nZVI were analyzed by FE-SEM and their results presented in Fig. 1. As observed in Fig. 1(a), the surface of PPAC has a highly porous structure, resulting in a high surface area for the adsorbent. In Fig. 1(b, c) white points on the surface of the adsorbent represent the nZVI and ZnO nanoparticles, which have an agglomeration structure and scattered abnormality. The size of nanoparticles was synthesized in the range of 19 to 24 nm. EDAX analysis was used to present the coating of nanoparticles on PPAC. As shown in Fig. 2(a), there are not any nZVI and ZnO ions on PPAC, however as shown in Fig. 2(b, d), nZVI and ZnO ions are coated on PPAC.

3.1.2. BET analysis

The N_2 adsorption-desorption isotherms and pore size distribution of PPAC–nZVI, PPAC–ZnO and PPAC at 77° K and a pressure range of 1–0, have been presented in Fig. S1. The results revealed that PPAC–nZVI, PPAC–ZnO and PPAC belong to type IV isotherm and H_2 type hysteresis loop. Pore size distribution analysis revealed that three synthesized adsorbents have mesoporous structures according to AUPAC classification (microspores if $Dp \leqslant 2$ nm, mesopores if $Dp = 2–50$ nm and macropores if $Dp \geqslant 50$ nm). Besides, BJH analysis was applied to further confirm the mesoporosity of PPAC–nZVI, PPAC–ZnO and PPAC. According to Table 1, the PPAC–nZVI, PPAC–ZnO and PPAC are mesoporous with a narrow pore size distribution centered at around 3 nm. By comparing Fig. S1, it can be found that the PPAC–nZVI composite have a greater porosity than the PPAC– ZnO and PPAC. The results obtained from analyzing the isotherm of PPAC– nZVI, PPAC– ZnO

Please cite this article as: Y. Rashtbari, S. Hazrati, A. Azari et al., A novel, eco-friendly and green synthesis of PPAC-ZnO and PPAC-nZVI nanocomposite using pomegranate peel: Cephalexin adsorption experiments, mechanisms, isotherms and kinetics, Advanced Powder Technology, https://doi.org/10.1016/j.apt.2020.02.001

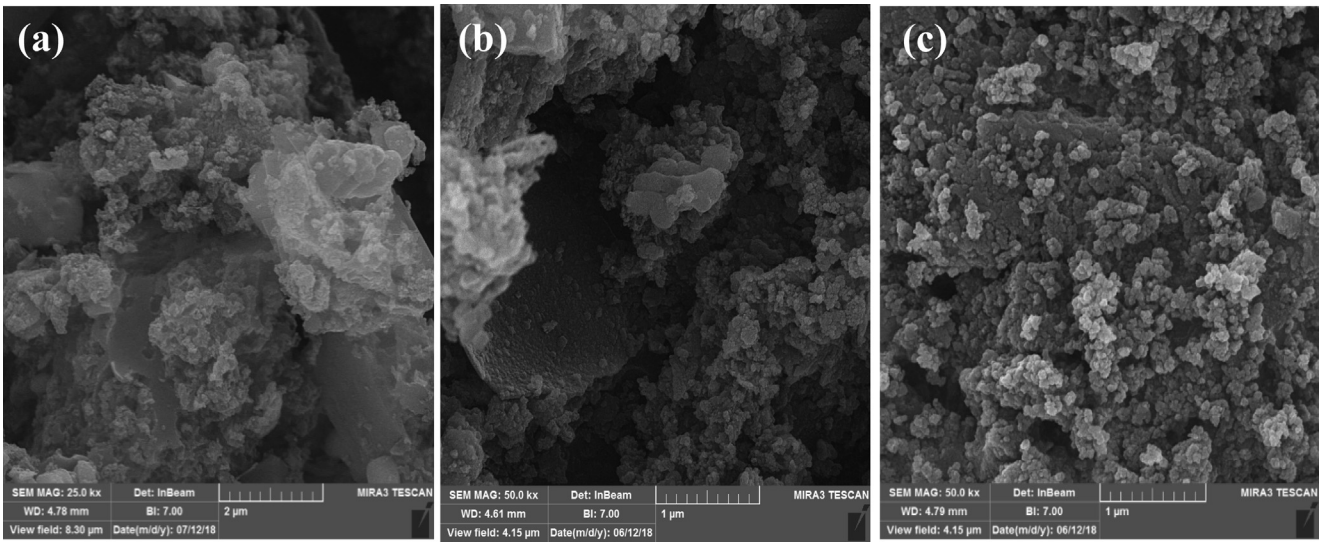

Fig. 1. FE-SEM images for PPAC (a) PPAC–nZVI (b) PPAC–ZnO (c).

and PPAC with BET analysis showed that the specific surface area of the prepared PPAC–nZVI, PPAC–ZnO and PPAC are 827.66 m^2 g^{-1}, 745.65 m^2 g^{-1} and 738.17 m^2 g^{-1} respectively. As well as, the PPAC– nZVI comprise a total pore volume of 0.6357 cm^3 g^{-1} that is larger than that of the PPAC– ZnO (0.6004 cm^3 g^{-1}) and PPAC (0.558 cm^3 g^{-1}). The results indicated that although some of the pores of activated carbon are blocked by the presence of NPs, the composites still has a large BET surface area and a high pore volume for a good adsorption. Furthermore, it is notable that the mesopore volume (Vmeso) significantly higher than micropore volume (Vmicro) in all samples. In fact, as can be seen in Table 1, PPAC–nZVI, PPAC–ZnO and PPAC exhibit similar mesopore volume (Vmeso) of around 0.3 cm^3 g^{-1}.

3.1.3. FTIR analysis

As it can be seen from FTIR spectrum in Fig. 3, the site of the majority of the bands existent in adsorbents' structure remains unchanged following nanoparticle loading and this signifies the preservation of adsorbents' structure following nanoparticle loading. The adsorption peak in 900–1300 cm^{-1} belongs to functional groups containing phosphorus pertinent to the adsorbent activation using phosphoric acid during the preparation process [14]. Peaks below 700 cm^{-1} pertain to Fe—O and Zn—O bonds vibrations. The presence of ZnO and nZVI nanoparticles can be proved with the emergence of two strong adsorption bands in 598–626 cm^{-1} [32,49]. The broad bands of PPAC-ZnO and PPAC-nZVI that are related to O—H vibrations in H_2O molecule appear in 3444–3427 cm^{-1}, respectively [50]. The existence of a peak in 2921–2948 cm^{-1} is indicative of the effects of C—H and O—H (with acidic origins) bonds in pomegranate skin extract on the nanoparticle formation [51]. Polyphenols, as the main factor of NPs' stabilization, are seen in 3200–3500 cm^{-1} range [52]. Some adsorption peaks disappear after ZnO and nZVI coating in PPAC and this causes reduction in perturbations. These results confirm the successful nZVI and ZnO coating in PPAC.

3.2. Effect of pH on CEX adsorption

The effect of pH on CEX removal were evaluated and the results are shown in Fig. 4. The highest removal was evidenced in pH = 5 for both PPAC-nZVI and PPAC-ZnO with 86.73% and 81.64% efficiency. The increase in pH to 11 causes reduction in removal efficiencies to 45.08% and 39.25% for PPAC-nZVI and PPAC-ZnO, respectively. Thus, the lowest and the highest removal were documented for pH values equal to 11 and 5. The relationship between CEX adsorption and solution pH can be influenced by composites surface load, functional groups on carbon, chemical structure and pK_a of cephalexin. Adsorption process efficiency depends on pH value because pH causes changes in adsorbent's surface load. In the present study, pH_{pzc} values equal to 6.83 and 6.42 were obtained for PPAC-ZnO and PPAC-nZVI, respectively. CEX possesses an amine group in its side chain as well as a carboxyl group. CEX features two PK_{a1} = 2.56 and PK_{a2} = 6.88 that are in anion form in pH = 6.88 and in action form in pH values below 2.56 and they are in molecular or charge-free forms in pH values between PK_{a1} and PK_{a2} amounts for the reason that the protons of the functional groups are lost [13]. In basic pH values, CEX molecules are dissolved in their anion forms. In addition, pH_{pzc} of the adsorbent's surface is surrounded by the carboxylic factors containing proton and H^+ ion and such conditions cause an increase in positive charge of the composite surface. In pH values higher than pH_{pzc}, the functional groups on the composite surface lose proton in the presence of OH^- ions hence they will have more negative charges as a result of which in pH values lower than pH_{pzc}, the majority of dominant cephalexin species feature negative charges and a little positive charge in the solution; whereas, in this pH domain, the adsorbent's surface takes positive charges. So, the electrostatic attraction between the negatively charged cephalexin molecules and positive adsorbent surface causes an increase in the adsorption output following which the adsorbent's surface will be negatively charged due to the high concentration of OH^- ions when the pH of the solution is increased upon reaching values about 11 hence the efficiency of adsorption process is subsequently reduced [5,53,54]. In the study by Ming-Sheng Miao et al. (2016) who used zero iron nanoparticles for removing CEX antibiotics by active carbon, the optimum CEX solution pH was set at 5.1 [14]. Zero iron nanoparticles were used in a study by Hassani et al for removing CEX antibiotics from aqueous environments and it was shown in the results that the increase in pH leads in reduction in CEX antibiotics removal output [55]. Additionally, in another study, Lengoverde et al utilized SAB15 mesopores for the removal of CEX antibiotics from aqueous environments and the results of their study indicated that the highest absorption of the antibiotic occurs in acidic pH [56].

Please cite this article as: Y. Rashtbari, S. Hazrati, A. Azari et al., A novel, eco-friendly and green synthesis of PPAC-ZnO and PPAC-nZVI nanocomposite using pomegranate peel: Cephalexin adsorption experiments, mechanisms, isotherms and kinetics, Advanced Powder Technology, https://doi.org/10.1016/j.apt.2020.02.001

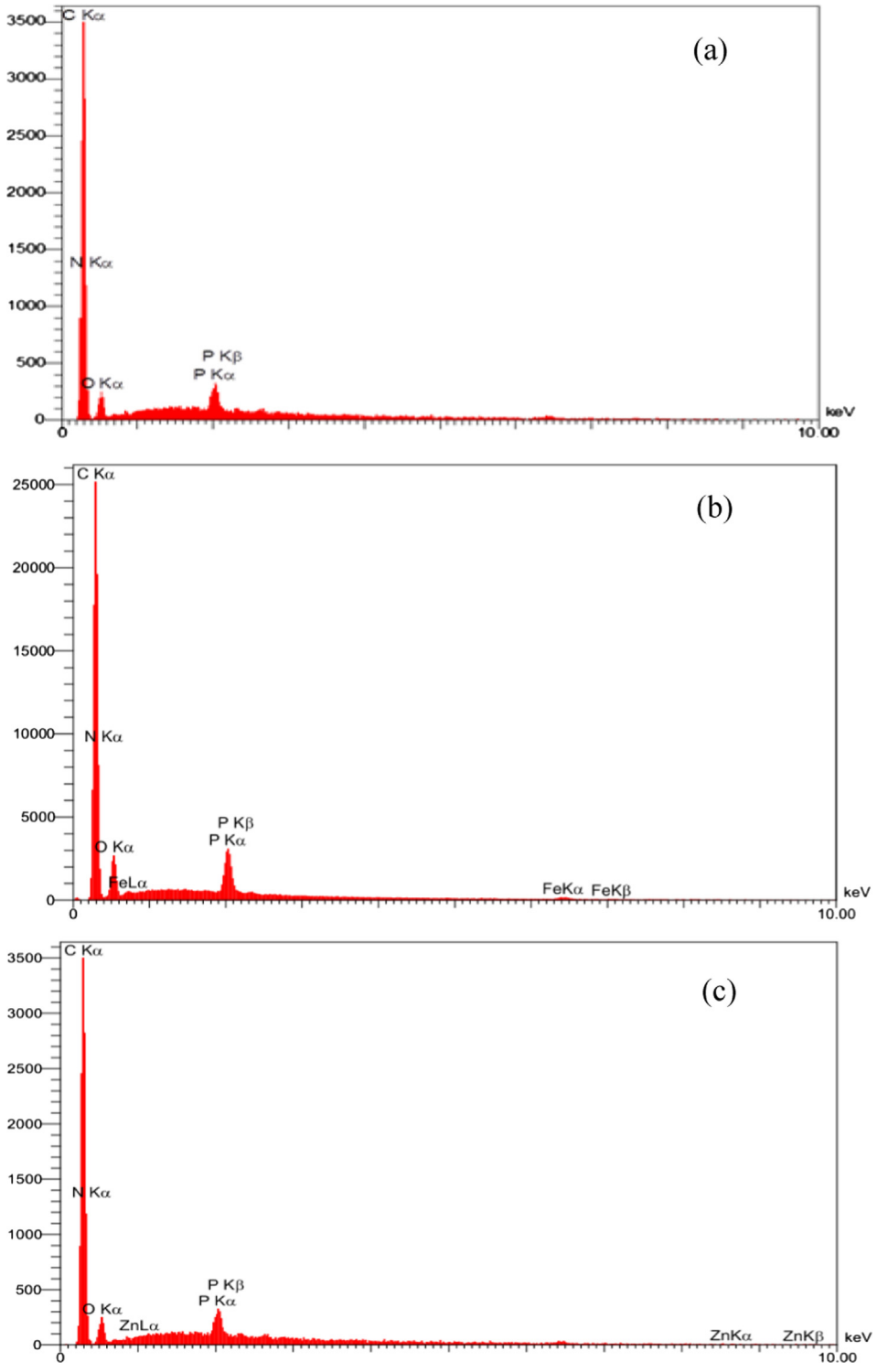

Fig. 2. EDAX spectra for PPAC (a), PPAC–nZVI (b) and PPAC–ZnO (c).

Table 1
Porous structure parameters of the three activated carbon samples.

Material	$S_{BET}(m^2g^{-1})$	$S_{micro}(m^2g^{-1})$	$S_{meso}(m^2g^{-1})$	$V_{Total}(cm^3g^{-1})$	$V_{micro}(cm^3g^{-1})$	$V_{meso}(cm^3g^{-1})$	D_p
PPAC	738.17	525.53	212.64	0.558	0.2328	0.3252	3.0237
PPAC-ZnO	745.65	513.07	212.58	0.6004	0.1372	0.368	3.3097
PPAC- nZVI	827.66	596.06	231.6	0.6357	0.2689	0.3668	3.0721

*Specific surface area (S_{BET}), Micropore specific surface area (S_{micro}), Mesopore specific surface area (S_{meso}), Total pore volume (V_{Total}), Micropore volume (V_{micro}), Mesopore volume (V_{meso}), Average pore diameter or Pore size distribution (D_p).

Please cite this article as: Y. Rashtbari, S. Hazrati, A. Azari et al., A novel, eco-friendly and green synthesis of PPAC-ZnO and PPAC-nZVI nanocomposite using pomegranate peel: Cephalexin adsorption experiments, mechanisms, isotherms and kinetics, Advanced Powder Technology, https://doi.org/10.1016/j.apt.2020.02.001

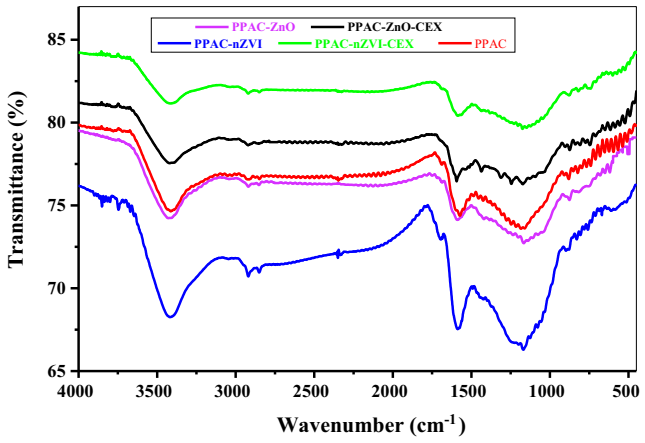

Fig. 3. FTIR spectra of the three synthesized adsorbents before and after CEX removal.

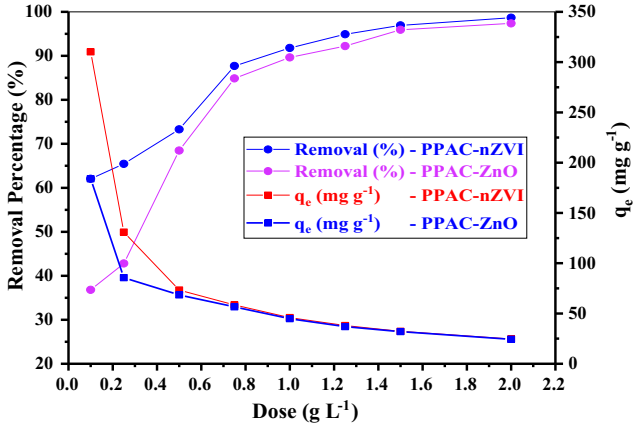

Fig. 5. Effect of adsorbent dose on the adsorption of CEX by PPAC-ZnO and PPAC-nZVI (initial concentration = 50 mg L^{-1}, pH = 5, contact time = 30 min).

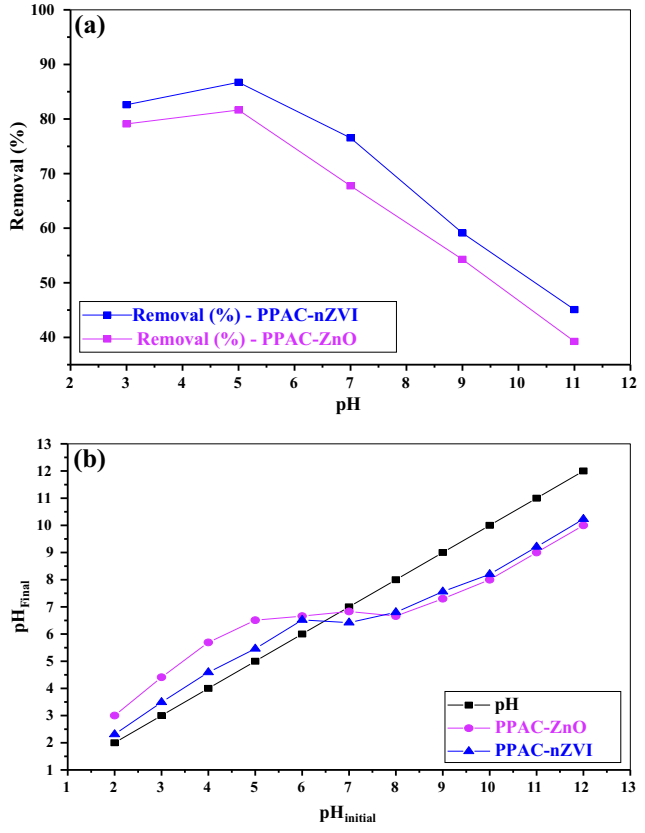

Fig. 4. The effect of solution pH on the CEX removal by PPAC-ZnO and PPAC-nZVI (initial concentration = 50 mg L^{-1}, dose = 0.75 g L^{-1}, and contact time = 30 min) [53,54,56–60] (a) and pH_{pzc} of PPAC-ZnO and PPAC-nZVI (b).

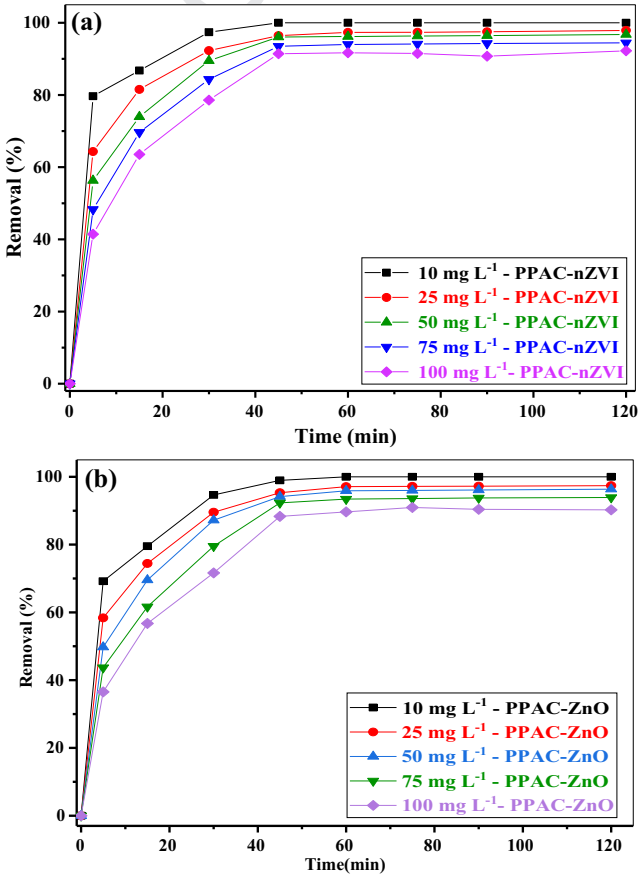

Fig. 6. Effect of contact time on CEX adsorption onto PPAC-nZVI (a) and PPAC-ZnO (b) (adsorbent concentration = 1.25 g L^{-1}, pH = 5, shaking speed = 250 rpm at room temperature).

3.3. Effect of adsorbent dosage on CEX adsorption

The effect of adsorbent dosage on removal of CEX is shown in Fig. 5. In this study the adsorbent dose was varied from 0.1 to 2 g L^{-1} under optimum conditions resulted from the previous tests. As seen in Fig. 5 adsorption capacity decreases (q_e) remarkably with increase in adsorbent dosage. With the increase in the adsorbent dosage from 0.1 to 2 g L^{-1}, the removal efficiency of CEX was also increased but it has little impact in higher dosages possibly due to the aggregation of NPs and decrease in the number of available binding sites, so, 1.25 g L^{-1} was selected as the optimum value for further study. In study by Miao et al. for removal of CEX from effluent by activated carbon derived from alligator weed, it was done, the results showed that the effect of removal of CEX with increasing dose of adsorbent increased to a certain amount and then its amount was constant [14]. This enhancement could be due mainly to the increase in surface area and adsorption sites with increasing adsorbent dose [58].

Please cite this article as: Y. Rashtbari, S. Hazrati, A. Azari et al., A novel, eco-friendly and green synthesis of PPAC-ZnO and PPAC-nZVI nanocomposite using pomegranate peel: Cephalexin adsorption experiments, mechanisms, isotherms and kinetics, Advanced Powder Technology, https://doi.org/10.1016/j.apt.2020.02.001

Table 2
Adsorption kinetic of CEX onto PPAC-nZVI and PPAC-ZnO and non-linear adjustments of the kinetic models (T = 298 ± 0.5 K; 250 rpm, 5–120 min).

	Initial concentration				
	10 mg L^{-1}	25 mg L^{-1}	50 mg L^{-1}	75 mg L^{-1}	100 mg L^{-1}
	PPAC-nZVI				
Pseudo-first order					
q_e (mg g^{-1})	7.47	19.09	37.86	55.67	72.57
k_1 (min^{-1})	0.38	0.20	0.14	0.11	0.09
h_0 (mg g^{-1} min^{-1})	2.82	3.84	5.49	6.37	6.63
R^2	0.990	0.985	0.978	0.983	0.984
RMSE	0.24	0.79	1.93	2.54	3.26
Pseudo-second order					
q_e (mg g^{-1})	7.68	20.23	40.75	60.76	80.42
k_2 (min^{-1})	0.11	0.016	0.006	0.003	0.002
h_0 (mg g^{-1} min^{-1})	6.80	6.76	9.28	10.45	10.61
R^2	0.997	0.998	0.995	0.996	0.993
RMSE	0.13	0.26	0.93	1.27	2.19
Elovich					
α (mg g^{-1} min^{-1})	1.77×10^5	243.80	92.71	56.03	37.66
β (g mg^{-1})	2.26	0.46	0.18	0.11	0.07
R^2	0.999	0.989	0.984	0.981	0.977
RMSE	0.03	0.67	1.64	2.66	3.89
	AC-ZnO				
Pseudo-first order					
q_e (mg g^{-1})	7.63	18.97	37.82	55.59	71.94
k_1 (min^{-1})	0.23	0.15	0.11	0.09	0.07
h_0 (mg g^{-1} min^{-1})	1.76	2.91	4.29	4.83	5.12
R^2	0.974	0.974	0.981	0.976	0.980
RMSE	0.41	1.05	1.82	3.02	3.62
Pseudo-second order					
q_e (mg g^{-1})	8.05	20.39	41.27	61.65	81.26
k_2 (min^{-1})	0.048	0.012	0.004	0.002	0.001
h_0 (mg g^{-1} min^{-1})	3.14	4.91	7.08	7.83	7.99
R^2	0.994	0.995	0.995	0.990	0.988
RMSE	0.21	0.48	0.94	1.99	2.74
Elovich					
α (mg g^{-1} min^{-1})	200.57	55.37	37.86	27.15	20.80
β (g mg^{-1})	1.26	0.38	0.16	0.09	0.06
R^2	0.992	0.987	0.982	0.979	0.977
RMSE	0.23	0.73	1.77	2.79	3.85

3.4. Effect of contact time and initial CEX concentration

The experiments for investigating the effect of contact time and initial CEX concentration were carried out by adding 1.25 gL^{-1} of the adsorbent into flasks contained the initial CEX concentration of 10, 25, 50, 75 and 100 mg L^{-1}. Fig. 6(a) and (b) shows the effect of contact time ranged from 5 to 120 min and initial CEX concentration on its removal by adsorbent from synthetic aqueous solutions at 25 °C. The adsorption of CEX was very fast in the first 30 min and then declined slowly with time until reaching the equilibrium. Hence, it is remarkable that the CEX reached completely equilibrium within only 45 min. Further increase in the contact time beyond 45 min did not enhance the adsorption efficiency and the variation of removal efficiency remained negligible. Therefore, this time was considered as the equilibrium and used in the experiments. The rapid removal efficiency in the beginning can be attributed to the higher concentration of pollutant molecules making higher driving force and the availability of more surface area on the adsorbent [13]. Subsequently, the CEX molecule enter into the pores (interior surface) and a relatively slow process is due to slow pore diffusion of the solute ions into the bulk of the adsorbents [59]. The results are consistent with other studies [48,60].

3.5. Adsorption kinetics

The effect of contact time on the adsorption of CEX onto PPAC-ZnO and PPAC-NZVI was studied with various initial CEX concentrations (10, 25, 50, 75 and 100 mg L^{-1}), adsorbate dose = 1.25 g L^{-1} and pH = 5. As shown in Fig. 6, it is clear that the adsorption rate of CEX was rapidly increased initially and gradually increased until equilibrium was reached. At the beginning of adsorption process, the high concentrations of CEX molecules (as driving force) in solution and the availability of huge vacant active sites on the adsorbents surface resulted in significant adsorption rates. After a given time, the decrease of CEX molecules adsorption and vacant binding sites probably led to negligible increase in the adsorption of CEX with time [61,62].

In order to find the best kinetic model describing the adsorption of CEX onto PPAC-ZnO and PPAC-NZVI, the Pseudo-first order, Pseudo-second order and Elovich kinetic models were nonlinearly fitted to experimental data (Fig. S2). As can be seen from the Table 2, the pseudo-first order kinetic described the experimental data obtained at low CEX concentrations better than those of high concentrations. This indicate that, at low initial concentrations, the number of free sites present onto both adsorbents was significantly greater than the number of CEX molecules adsorbed.

Overall, all kinetic models showed high R^2 values and low RMSE, indicating good fits to the experimental data. At the initial CEX concentrations of 10 mg L^{-1}, the Elovich model showed the better fit, indicating that the process occurred by chemical adsorption on the energetically heterogeneous surface of both adsorbents. At higher initial CEX concentrations, the kinetics well described by the pseudo-second order model. This implies that the rates of CEX adsorption onto PPAC-nZVI and PPAC-ZnO were controlled by chemisorption.

It is well known that the values of h_0 (in pseudo-first and -second order kinetics) and α (in Elovich model) correspond to the initial adsorption rate [63]. The higher h_0 and α values, the faster the initial adsorption rate. According to the values of these parameters which presented in Table 2, the initial adsorption rate

Please cite this article as: Y. Rashtbari, S. Hazrati, A. Azari et al., A novel, eco-friendly and green synthesis of PPAC-ZnO and PPAC-nZVI nanocomposite using pomegranate peel: Cephalexin adsorption experiments, mechanisms, isotherms and kinetics, Advanced Powder Technology, https://doi.org/10.1016/j.apt.2020.02.001

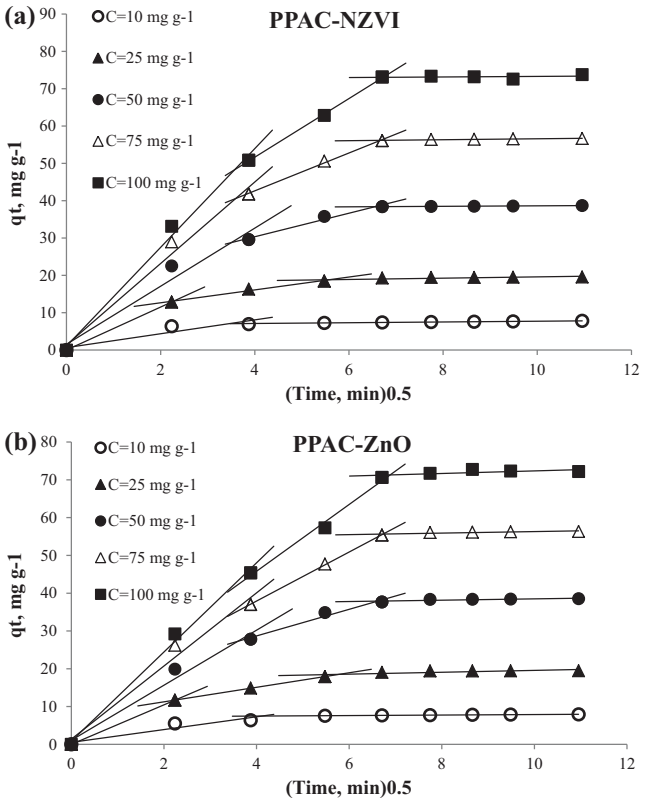

Fig. 7. Intraparticle diffusion plots for the adsorption of CEX onto PPAC-nZVI and PPAC-ZnO.

of CEX onto PPAC-nZVI was higher than that observed for cephalexin/PPAC-ZnO system. Therefore, it seems that the higher S_{BET} of PPAC-nZVI probably provided more vacant sites, compared to that of PPAC-ZnO, for CEX adsorption at the beginning of adsorption process.

The Intraparticle diffusion model proposed by Weber and Morris (1963) was used in order to describe how the diffusion of CEX molecules onto PPAC-ZnO and PPAC-nZVI takes place [64]. This model assumes that the adsorption phenomenon occurs in three sequential stages: the external diffusion of the adsorbate through the liquid film layer on the external surface of the sorbent, (ii) the Intraparticle or pore diffusion of the adsorbent through the internal surface of sorbent, and (iii) the adsorption of adsorbate molecules on the active sites of the adsorbent surface [65].

The values of characteristic parameters in the Intraparticle diffusion model, K_{id} and C_i, were determined through plotting q_t versus $t^{0.5}$ (Fig. 7) and listed in Table 3. As shown in Fig. 7, except for the fit of 10 mg L^{-1} kinetic, three defined stages were observed in the graphs. The first sharp stage represents the instantaneous adsorption and external diffusion of the antibiotic molecules from solution to the outer surface of the adsorbents. The second linear stage, which was not observed in the concentration of 10 mg L^{-1}, can be attributed to the penetration of CEX molecules into interlayer of the adsorbents where Intraparticle diffusion is rate limiting. The third flat stage corresponds to the adsorption equilibrium. From Fig. 7, it can be inferred that the lines did not pass through the origin, indicating that the Intraparticle diffusion was not the only rate limiting mechanism in the adsorption process; thus, some other mechanisms like liquid film diffusion may influence the adsorption kinetics.

The slope of the plots, K_{id}, characterizes the adsorption rate in Intraparticle diffusion model. According to Table 4, the values of K_{id} were in the order of $K_{id,1} > K_{id,2} > K_{id,3}$. Such trends indicates that the rate of CEX adsorption was initially faster and then slowed down, probably due to availability of more vacant adsorption sites at the beginning of adsorption process. The intercept of the second stage plots, C_2, provides an insight into the tendency of the adsorbate to be adsorbed onto the adsorbent or remain in solution. As is explicit from Table 3, the values of C_2 were greater in Cephalexin/PPAC-nZVI compared to those of Cephalexin/PPAC-ZnO system, depicting more tendency of PPAC-nZVI surface to the CEX molecules.

Table 4
Parameters of isotherm models for the adsorption of CEX onto PPAC-nZVI and PPAC-ZnO.

	PPAC-nZVI	PPAC-ZnO
Freudlich		
k_F (mg g^{-1})	39.49	37.38
n_F	5.79	5.84
$1/n_F$	0.17	0.17
R^2	0.880	0.879
RMSE	10.64	10.06
Langmuir		
q_m (mg g^{-1})	87.18	82.60
k_L (L mg^{-1})	0.49	0.44
R^2	0.986	0.985
RMSE	2.05	1.78
Redlich-Peterson		
a_{RP} (L $mg^{-1})^{-g}$	37.60	31.97
b_{RP} (L g^{-1})	0.38	0.34
g	1.03	1.03
R^2	0.987	0.987
RMSE	3.46	3.33
Temkin		
b_T	211.31	222.47
k_T	19.15	17.84
R2	0.927	0.926
RMSE	8.38	7.86

Table 3
Parameters of intraparticle diffusion kinetic for the adsorption of CEX onto PPAC-ZnO and PPAC-NZVI.

	Time	First stage		Second stage		Third stage	
		$K_{id,1}$ (mg g^{-1} $min^{-0.5}$)	C_1 (mg g^{-1})	$K_{id,2}$	C_2	$K_{id,3}$	C_3
PPAC-nZVI	10	1.85	0.66	–	–	0.10	6.73
	25	5.75	3×10^{-15}	1.73	9.21	0.17	17.88
	50	7.78	1.52	3.15	17.73	0.07	37.96
	75	10.92	1.35	5.07	22.38	0.13	55.34
	100	13.23	1.06	7.84	20.27	0.08	72.56
PPAC-ZnO	10	1.69	0.52	–	–	0.07	7.21
	25	5.22	1×10^{-15}	1.92	7.39	0.25	17.09
	50	7.29	1.07	3.52	14.63	0.18	36.74
	75	9.68	1.36	6.49	11.95	0.20	54.28
	100	11.80	0.85	8.84	10.46	0.34	68.96

Please cite this article as: Y. Rashtbari, S. Hazrati, A. Azari et al., A novel, eco-friendly and green synthesis of PPAC-ZnO and PPAC-nZVI nanocomposite using pomegranate peel: Cephalexin adsorption experiments, mechanisms, isotherms and kinetics, Advanced Powder Technology, https://doi.org/10.1016/j.apt.2020.02.001

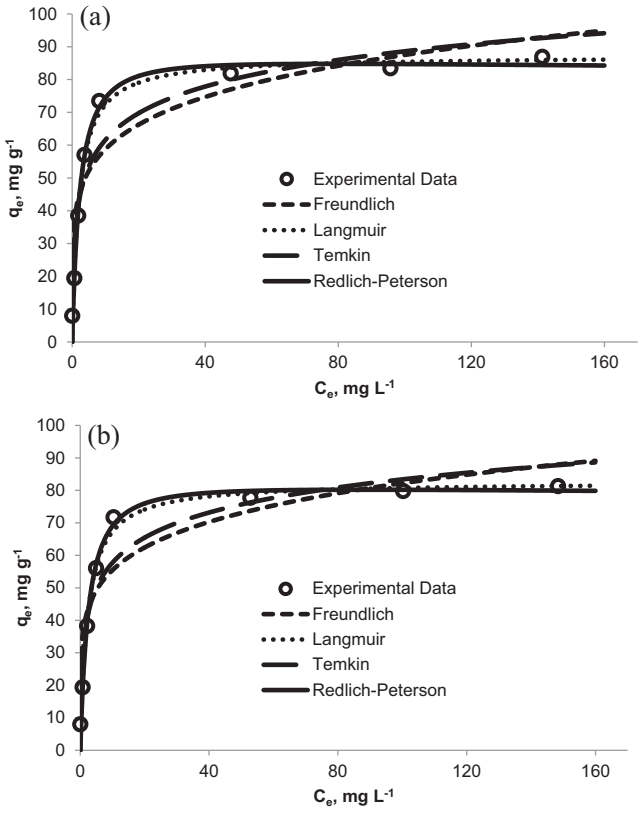

Fig. 8. Isotherm models fitted to the Cephalexin adsorption onto PPAC-nZVI (a) and PPAC-ZnO (b).

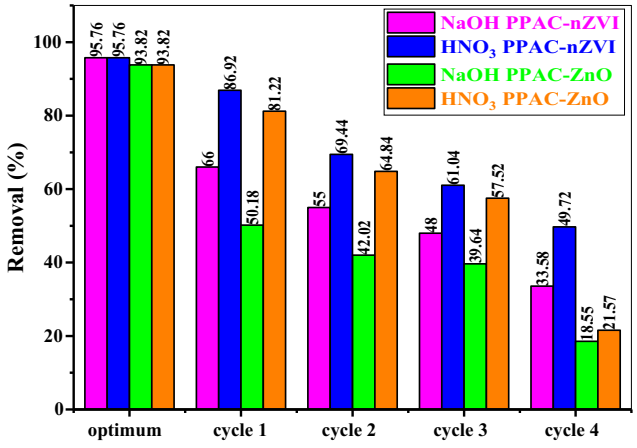

Fig. 9. Adsorption–desorption cycles of PPAC-ZnO and PPAC-nZVI.

3.6. Isotherm studies

Adsorption isotherms provide valuable information for analyzing and designing an adsorption process. Four common isotherm models, i.e. Freundlich, Langmuir, Redlich-Peterson and Temkin were applied to describe the experimental data of equilibrium CEX adsorption onto PPAC-ZnO and PPAC-nZVI.

The Freundlich isotherm shows that the adsorption occurs on a heterogeneous surface by multilayer adsorption, while Langmuir isotherm describe uniform monolayer adsorption onto a surface containing a finite number of adsorption sites [66,67]. The Redlich-Peterson isotherm is a hybrid isotherm, in which both Freundlich and Langmuir features are combined. Temkin model assumes that the adsorption heat increases linearly with the coverage of adsorbent [63].

The nonlinear fits of the isotherm models to the experimental data of CEX adsorption onto PPAC-ZNO and PPAC-nZVI are presented in Fig. 8 and their parameters along with R^2 and RMSE values are presented in Table 4.

The according to the R^2 and RMSE values, Redlich-Peterson model best described the experimental data of CEX adsorption onto both adsorbents, considering its highest R^2 and the low value of RMSE. This isotherm model is applied to show the adsorption equilibrium in a wide range of adsorbate concentrations in homogeneous and heterogeneous systems according to their compatibility.

This isotherm consists of the combination of the Langmuir and Freundlich models, which are distinguished by the exponent g. The value of g in this model lies between 0 and 1. When the value of g tends to 1, the isotherm behaves according to the Langmuir isotherm. In the other hand, for $g < 1$ and the values of a_{RP} and b_{RP} parameters above 1, the isotherm resembles the Freundlich approach.

Regarding the values of g, a_{RP} and b_{RP} parameters in Table 4, it can be implied that the CEX adsorption onto both adsorbents described better by the Langmuir approach than by the Freundlich one. Therefore, the isotherm modeling implied the adsorption of CEX onto PPACs was occurred in monolayer.

The separation factor (R_L) in the Langmuir model was used to determine if the adsorption process is irreversible ($R_L = 0$), linear ($R_L = 1$), favorable ($0 < R_L < 1$), or unfavorable ($R_L > 1$) [68]. For the range of applied initial CEX concentrations (10–100 mg L^{-1}), the R_L values decreased from 0.3784 to 0.0149 for Cephalexin/PPAC-ZnO system and from 0.0599 to 0.0015 for Cephalexin/PPAC-nZVI system, indicating the favorability of CEX adsorption onto both adsorbents in the concentration range studied.

The maximum monolayer adsorption capacities (q_m) for PPAC-ZnO and PPAC-nZVI were 82.60 and 87.18 mg g^{-1}, respectively, which are considerable compared to those reported for several biomass-derived PPACs applied for Cephalexin adsorption (Table S2). The isotherm study showed that CEX was more favorably adsorbed onto PPAC-nZVI than that of PPAC-ZnO. Moreover, the maximum monolayer adsorption capacity of PPAC-nZVI was higher than that of PPAC-ZnO. Therefore, the PPAC-nZVI, probably due to higher content of oxygen functional groups, higher specific surface area and higher pore volume, showed better potential for the adsorption of CEX. Moreover, the proportion of mesoporous in PPAC-nZVI (72.01%) was higher than that of PPAC-ZnO (68.8%) (Table 1).

3.7. Regeneration of PPAC-ZnO and PPAC-nZVI

The regeneration ability of an adsorbent is an useful factor for evaluation of its commercial application [69]. Generally, chemical treatments are the most common methods for the regeneration of an exhausted adsorbent. In chemical regeneration, generally, CEX molecules are dissolved in the eluent or removed from the adsorbent biding sites by ion-exchange process [70]. The effect of NaOH and HNO_3 solution and the adsorption-regeneration cycle was studied in the recovery of the PPAC-ZnO and PPAC- nZVI after removal of CEX (Fig. 9). In the first stage, 1.25 g L^{-1} of PPAC-ZnO and PPAC-nZVI were added in 50 mgL^{-1} of CEX solution in optimum conditions and after the equilibrium time, the regeneration was investigated. The regeneration process was carried out up to five times. After the regeneration, the spent adsorbents for the next regeneration stage were dried at 100 °C for 12 h. Generally, it can be observed that the adsorption efficiency of the composite decreases as the number of regeneration cycle increases [71,72].

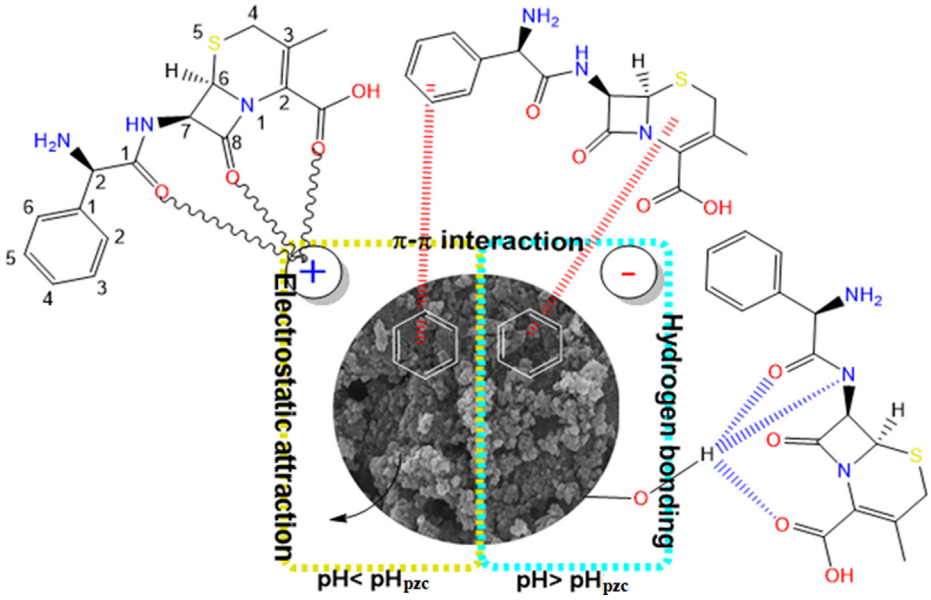

Fig. 10. Adsorption mechanism of CEX.

The PPAC-ZnO regeneration by 0.1 M NaOH and 0.1 M HNO_3 was able to maintain an elimination efficiency of about 18.5% and 25.41% and PPAC-nZVI equaled 33.58% and 49.72%, respectively, even after the fifth cycle. This can be justified because the high concentration of hydroxide ions and HNO_3 will compete with the species of antibiotics (CEX) which site on the active sites. The CEX is isolated from the active sites and the sorbent is regenerated [73]. Thus, it can be concluded from this experiment that PPAC-ZnO and PPAC-nZVI has high potential to be used in wastewater treatment of CEX since it can be reused by regeneration the adsorbent and coupled with its ability at maintaining great removal efficiency after five consecutive cycles, it may will be cost effectiveness [74].

3.8. Real wastewater samples

CEX removal by PPAC-nZVI and PPAC-ZnO was 69.78 and 66.32%, respectively. As it can be seen, the removal output of PPAC-nZVI and PPAC-ZnO composites is lower in real wastewater than in synthetic wastewater. This output reduction might be attributable to a higher pH and presence of soluble organic materials in the real samples both of which are known to influence CEX adsorption behavior [75]. Generally, these results are suggestive of the appropriate performance of composite in CEX removal from the real samples.

3.9. Adsorption mechanism

Based on the FTIR spectra, and changes (minor shifts after adsorption process) in phenolic O—H peaks, aromatic C=C bonds and alkoxy C—O bonds can be suggested that oxygen-containing functional groups of adsorbents, including phenolic hydroxyl group, carboxyl and alkoxy groups, were participated in adsorption of CEX. Thus, several possible interactions could describe the adsorption mechanisms of CEX onto the PPAC-nZVI and PPAC-ZnO as adsorbent. As shown in Fig. 10, three dominant mechanisms are recognizable in adsorption of CEX onto the nanocomposites, (i) π–π interaction between adsorbents surface and the antibiotic (ii) electrostatic attraction between adsorbent and adsorbate and finally (iii) hydrogen bonding interaction.

Indeed, the π–π interaction is established between sp2-hybridized domains of adsorbents and aromatic structure of CEX, electrostatic attraction is established between negatively charged of CEX and positive charge present on the surface of PPAC-nZVI and PPAC-ZnO (at pH < pHpzc, the adsorbent surface has a positive charge) and for pH values > pHpzc that adsorbents surface has a negative charge, H-bond (hydrogen bonding) between antibiotic and a surface carboxylate or phenolate may attribute to the adsorption.

4. Conclusions

Pomegranate peel and H_3PO_4 were exposed to an ultrasonic process to obtain PPAC-ZnO and PPAC-nZVI, and which were applied as efficient adsorbent for removal of CEX from aqueous solution. The surface areas of PPAC-ZnO and PPAC-nZVI were 738.17 and 827.66 $m^2\ g^{-1}$ and the total pore volume are 0.558 and 0.6357 $cm^3\ g^{-1}$. Adsorption studies of CEX onto PPAC-ZnO and PPAC-nZVI indicated that the kinetic model of pseudo-second-order and the adsorption isotherm model of Langmuir fitted well to the obtained data. These models represented that the adsorption process may occurs by chemisorption and takes place as monolayer adsorption. The optimum conditions in the present research were determined at pH = 5, contact time = 45 min and adsorbent dosage = 1.25 gL^{-1}. The maximum adsorption capacity followed an order of PPAC–nZVI (87.18 mg g^{-1}) > PPAC-ZnO (82.6 mg g^{-1}) which was corresponding to the BET results, indicating the adsorption of CEX onto the two adsorbents had a significant relationship with the porosity of activated carbons. Moreover, extract of pomegranate peel was an efficient candidate for the synthesis of nZVI and ZnO NPs. Regeneration experiment showed PPAC-ZnO and PPAC-nZVI were stable for CEX removal; however, the regeneration efficiencies of PPAC– nZVI were a little higher than those of PPAC-ZnO. This study provided an environmentally friendly, low-cost adsorbent for the removal of CEX in wastewater.

Contributors

Sadegh Hazrati and Yousef Rashtbari participated in the conceptualization and design of the research and supervised the work. Ali Azari and Shirin Afshin are responsible for experimental analysis and interpretation of data. Mehdi Fazlzadeh and Mehdi

Please cite this article as: Y. Rashtbari, S. Hazrati, A. Azari et al., A novel, eco-friendly and green synthesis of PPAC-ZnO and PPAC-nZVI nanocomposite using pomegranate peel: Cephalexin adsorption experiments, mechanisms, isotherms and kinetics, Advanced Powder Technology, https://doi.org/10.1016/j.apt.2020.02.001

Vosoughi wrote the first draft of manuscript. All authors have read and approved the final paper as submitted.

Acknowledgments

The authors would like to acknowledge Ardabil University of Medical Sciences for financial and instrumental supports (code: IR.ARUMS.REC.1396.119).

Appendix A. Supplementary material

Supplementary data to this article can be found online at https://doi.org/10.1016/j.apt.2020.02.001.

References

[1] M. Pirsaheb, H. Hossaini, H. Janjani, An overview on ultraviolet persulfate based advances oxidation process for removal of antibiotics from aqueous solutions: a systematic review, Desalination Water Treat. 165 (2019) 382–395.
[2] S.A. Mousavi, H. Janjani, Antibiotics adsorption from aqueous solutions using carbon nanotubes: a systematic review, Toxin Rev. (2018) 1–12.
[3] A. Dehghan, A. Zarei, J. Jaafari, M. Shams, A.M. Khaneghah, Tetracycline removal from aqueous solutions using zeolitic imidazolate frameworks with different morphologies: A mathematical modeling, Chemosphere 217 (2019) 250–260.
[4] R. Khosravi, A. Zarei, M. Heidari, A. Ahmadfazeli, M. Vosughi, M. Fazlzadeh, Application of ZnO and TiO 2 nanoparticles coated onto montmorillonite in the presence of H 2 O 2 for efficient removal of cephalexin from aqueous solutions, Korean J. Chem. Eng. 35 (2018) 1000–1008.
[5] W. Liu, H. Xie, J. Zhang, C. Zhang, Sorption removal of cephalexin by HNO 3 and H 2 O 2 oxidized activated carbons, Sci. China Chem. 55 (2012) 1959–1967.
[6] A.R. Rahmania, A. Shabanlooa, M. Fazlzadehb, Y. Poureshghd, M. Vanaeitabara, Optimization of sonochemical decomposition of ciprofloxacin antibiotic in US/PS/nZVI process by CCD-RSM method, Desalination Water Treat. 145 (2019) 300–308.
[7] R. Shokoohi, M.T. Samadi, M. Amani, Y. Poureshgh, Optimizing laccase-mediated amoxicillin removal by the use of box–behnken design in an aqueous solution, Desalin. Water Treat. 119 (2018) 53–63.
[8] R. Shokoohi, M.T. Samadi, M. Amani, Y. Poureshgh, Modeling and optimization of removal of cefalexin from aquatic solutions by enzymatic oxidation using experimental design, Braz. J. Chem. Eng. 35 (2018) 943–956.
[9] M. Leili, M. Fazlzadeh, A. Bhatnagar, Green synthesis of nano-zero-valent iron from Nettle and Thyme leaf extracts and their application for the removal of cephalexin antibiotic from aqueous solutions, Environ. Technol. 39 (2018) 1158–1172.
[10] Y. Ji, C. Ferronato, A. Salvador, X. Yang, J.-M. Chovelon, Degradation of ciprofloxacin and sulfamethoxazole by ferrous-activated persulfate: Implications for remediation of groundwater contaminated by antibiotics, Sci. Total Environ. 472 (2014) 800–808.
[11] W. Liu, H. Xie, J. Zhang, C. Zhang, Sorption removal of cephalexin by HNO3 and H2O2 oxidized activated carbons, Sci. China Chem. 55 (2012) 1959–1967.
[12] Z. Li, H. Hong, L. Liao, C.J. Ackley, L.A. Schulz, R.A. MacDonald, A.L. Mihelich, S. M. Emard, A mechanistic study of ciprofloxacin removal by kaolinite, Colloids Surf. B. Biointerfaces 88 (2011) 339–344.
[13] H. Liu, W. Liu, J. Zhang, C. Zhang, L. Ren, Y. Li, Removal of cephalexin from aqueous solutions by original and Cu (II)/Fe (III) impregnated activated carbons developed from lotus stalks Kinetics and equilibrium studies, J. Hazard. Mater. 185 (2011) 1528–1535.
[14] M.-S. Miao, Q. Liu, L. Shu, Z. Wang, Y.-Z. Liu, Q. Kong, Removal of cephalexin from effluent by activated carbon prepared from alligator weed: Kinetics, isotherms, and thermodynamic analyses, Process Saf. Environ. Prot. 104 (2016) 481–489.
[15] M. Zazouli, M. Ulbricht, S. Nasseri, H. Susanto, Effect of hydrophilic and hydrophobic organic matter on amoxicillin and cephalexin residuals rejection from water by nanofiltration, J. Environ. Health Sci. Eng. 7 (2010) 15–24.
[16] A.A. Al-Gheethi, I. Norli, J. Lalung, A.M. Azlan, Z.N. Farehah, M.O.A. Kadir, Biosorption of heavy metals and cephalexin from secondary effluents by tolerant bacteria, Clean Technol. Environ. Policy 16 (2014) 137–148.
[17] W. Guo, H. Wang, Y. Shi, G. Zhang, Sonochemical degradation of the antibiotic cephalexin in aqueous solution, Water Sa 36 (2010).
[18] A.L. Estrada, Y.-Y. Li, A. Wang, Biodegradability enhancement of wastewater containing cefalexin by means of the electro-Fenton oxidation process, J. Hazard. Mater. 227 (2012) 41–48.
[19] V. Gabet-Giraud, C. Miège, J. Choubert, S.M. Ruel, M. Coquery, Occurrence and removal of estrogens and beta blockers by various processes in wastewater treatment plants, Sci. Total Environ. 408 (2010) 4257–4269.
[20] C. Jung, J. Heo, J. Han, N. Her, S.-J. Lee, J. Oh, J. Ryu, Y. Yoon, Hexavalent chromium removal by various adsorbents: powdered activated carbon, chitosan, and single/multi-walled carbon nanotubes, Sep. Purif. Technol. 106 (2013) 63–71.
[21] M. Ahmadian, M. Pirsaheb, H. Janjani, H. Hossaini, Ultraviolet activated persulfate based AOP for MTBE decomposition in aqueous solution, Desalin. Water Treat. 161 (2019) 269–274.
[22] R. Khosravi, H. Eslami, A. Zarei, M. Heidari, A.N. Baghani, N. Safavi, A. Mokammel, M. Fazlzadeh, S. Adhami, Comparative evaluation of nitrate adsorption from aqueous solutions using green and red local montmorillonite adsorbents, Desalin. Water Treat. 116 (2018) 119–128.
[23] M. Ghaedi, M. Ghayedi, S.N. Kokhdan, R. Sahraei, A. Daneshfar, Palladium, silver, and zinc oxide nanoparticles loaded on activated carbon as adsorbent for removal of bromophenol red from aqueous solution, J. Ind. Eng. Chem. 19 (2013) 1209–1217.
[24] M. Ghaedi, B. Sadeghian, A.A. Pebdani, R. Sahraei, A. Daneshfar, C. Duran, Kinetics, thermodynamics and equilibrium evaluation of direct yellow 12 removal by adsorption onto silver nanoparticles loaded activated carbon, Chem. Eng. J. 187 (2012) 133–141.
[25] W. Liu, J. Zhang, C. Zhang, L. Ren, Sorption of norfloxacin by lotus stalk-based activated carbon and iron-doped activated alumina: mechanisms, isotherms and kinetics, Chem. Eng. J. 171 (2011) 431–438.
[26] J. Kim, J. Kim, J.H. Kim, H.S. Park, Hierarchically open-porous nitrogen-incorporated carbon polyhedrons derived from metal-organic frameworks for improved CDI performance, Chem. Eng. J. 122996 (2019).
[27] J.H. Khan, F. Marpaung, C. Young, J. Lin, M.T. Islam, S.M. Alsheri, T. Ahamad, N. Alhokbany, K. Ariga, L.K. Shrestha, Jute-derived microporous/mesoporous carbon with ultra-high surface area using a chemical activation process, Microporous Mesoporous Mater. 274 (2019) 251–256.
[28] O.V. Kharissova, H.V.R. Dias, B.I. Kharisov, Magnetic adsorbents based on micro- and nano-structured materials, RSC Adv. 5 (2015) 6695–6719.
[29] I. Shah, R. Adnan, W.S. Wan Ngah, N. Mohamed, Iron impregnated activated carbon as an efficient adsorbent for the removal of methylene blue: regeneration and kinetics studies, PLoS ONE 10 (2015), e0122603-e0122603.
[30] S.J. Joshi, S. Geetha, S. Al-Mamari, A. Al-Azkawi, Green synthesis of silver nanoparticles using pomegranate peel extracts and its application in photocatalytic degradation of methylene blue, Jundishapur J. Nat. Pharm. Prod. 13 (2018).
[31] M. Çam, N.C. İçyer, F. Erdoğan, Pomegranate peel phenolics: microencapsulation, storage stability and potential ingredient for functional food development, LWT-Food Sci. Technol. 55 (2014) 117–123.
[32] O. Nava, C. Soto-Robles, C. Gómez-Gutiérrez, A. Vilchis-Nestor, A. Castro-Beltrán, A. Olivas, P. Luque, Fruit peel extract mediated green synthesis of zinc oxide nanoparticles, J. Mol. Struct. 1147 (2017) 1–6.
[33] M. Haghighi, F. Rahmani, R. Dehghani, A.M. Tehrani, M.B. Miranzadeh, Photocatalytic reduction of Cr (VI) in aqueous solution over ZnO/HZSM-5 nanocomposite: optimization of ZnO loading and process conditions, Water Treat 58 (2017) 168–180.
[34] Q.-S. Liu, T. Zheng, P. Wang, L. Guo, Preparation and characterization of activated carbon from bamboo by microwave-induced phosphoric acid activation, Ind. Crops Prod. 31 (2010) 233–238.
[35] L. Huang, X. Weng, Z. Chen, M. Megharaj, R. Naidu, Synthesis of iron-based nanoparticles using oolong tea extract for the degradation of malachite green, Spectrochim. Acta Part A Mol. Biomol. Spectrosc. 117 (2014) 801–804.
[36] T. Wang, J. Lin, Z. Chen, M. Megharaj, R. Naidu, Green synthesized iron nanoparticles by green tea and eucalyptus leaves extracts used for removal of nitrate in aqueous solution, J. Cleaner Prod. 83 (2014) 413–419.
[37] L. Huang, X. Weng, Z. Chen, M. Megharaj, R. Naidu, Green synthesis of iron nanoparticles by various tea extracts: Comparative study of the reactivity, Spectrochim. Acta Part A Mol. Biomol. Spectrosc. 130 (2014) 295–301.
[38] X. Weng, L. Huang, Z. Chen, M. Megharaj, R. Naidu, Synthesis of iron-based nanoparticles by green tea extract and their degradation of malachite, Ind. Crops Prod. 51 (2013) 342–347.
[39] T. Wang, X. Jin, Z. Chen, M. Megharaj, R. Naidu, Green synthesis of Fe nanoparticles using eucalyptus leaf extracts for treatment of eutrophic wastewater, Sci. Total Environ. 466–467 (2014) 210–213.
[40] M. Fazlzadeh, R. Khosravi, A. Zarei, Green synthesis of zinc oxide nanoparticles using Peganum harmala seed extract, and loaded on Peganum harmala seed powdered activated carbon as new adsorbent for removal of Cr (VI) from aqueous solution, Ecological Eng. 103 (2017) 180–190.
[41] E.M. Kalhori, K. Yetilmezsoy, N. Uygur, M. Zarrabi, R.M.A. Shmeis, Modeling of adsorption of toxic chromium on natural and surface modified lightweight expanded clay aggregate (LECA), Appl. Surf. Sci. 287 (2013) 428–442.
[42] Y. Rashtbari, S. Hazrati, S. Afshin, M. Fazlzadeh, M. Vosoughi, Data on cephalexin removal using powdered activated carbon (PPAC) derived from pomegranate peel, Data in Brief 20 (2018) 1434–1439.
[43] S. Afshin, S.A. Mokhtari, M. Vosoughi, H. Sadeghi, Y. Rashtbari, Data of adsorption of Basic Blue 41 dye from aqueous solutions by activated carbon prepared from filamentous algae, Data in Brief 21 (2018) 1008–1013.
[44] H. Abdoallahzadeh, B. Alizadeh, R. Khosravi, M. Fazlzadeh, Efficiency of EDTA modified nanoclay in removal of humic acid from aquatic solutions, J. Mazandaran Univ. Med. Sci. 26 (2016) 111–125.

[45] L. Sun, S. Wan, D. Yuan, Z. Yu, Adsorption of nitroimidazole antibiotics from aqueous solutions on self-shaping porous biomass carbon foam pellets derived from Vallisneria natans waste as a new adsorbent, Sci. Total Environ. (2019).
[46] C.P. Okoli, A.E. Ofomaja, Development of sustainable magnetic polyurethane polymer nanocomposite for abatement of tetracycline antibiotics aqueous pollution: Response surface methodology and adsorption dynamics, J. Cleaner Prod. (2019).
[47] M. Hadi, M.R. Samarghandi, G. McKay, Equilibrium two-parameter isotherms of acid dyes sorption by activated carbons: study of residual errors, Chem. Eng. J. 160 (2010) 408–416.
[48] M.R. Samarghandi, T.J. Al-Musawi, A. Mohseni-Bandpi, M. Zarrabi, Adsorption of cephalexin from aqueous solution using natural zeolite and zeolite coated with manganese oxide nanoparticles, J. Mol. Liq. 211 (2015) 431–441.
[49] P. Dorjee, D. Amarasiriwardena, B. Xing, Antimony adsorption by zero-valent iron nanoparticles (nZVI): Ion chromatography–inductively coupled plasma mass spectrometry (IC–ICP-MS) study, Microchem. J. 116 (2014) 15–23.
[50] L. Huang, S. Zhou, F. Jin, J. Huang, N. Bao, Characterization and mechanism analysis of activated carbon fiber felt-stabilized nanoscale zero-valent iron for the removal of Cr (VI) from aqueous solution, Colloids Surf., A 447 (2014) 59–66.
[51] K.S. Prasad, P. Gandhi, K. Selvaraj, Synthesis of green nano iron particles (GnIP) and their application in adsorptive removal of As (III) and As (V) from aqueous solution, Appl. Surf. Sci. 317 (2014) 1052–1059.
[52] M. Ramesh, M. Anbuvannan, G. Viruthagiri, Green synthesis of ZnO nanoparticles using Solanum nigrum leaf extract and their antibacterial activity, Spectrochim. Acta Part A Mol. Biomol. Spectrosc. 136 (2015) 864–870.
[53] M. Dutta, N. Dutta, K. Bhattacharya, Aqueous phase adsorption of certain beta-lactam antibiotics onto polymeric resins and activated carbon, Sep. Purif. Technol. 16 (1999) 213–224.
[54] K.Y. Wang, T.-S. Chung, The characterization of flat composite nanofiltration membranes and their applications in the separation of cephalexin, J. Membr. Sci. 247 (2005) 37–50.
[55] A. Hassani, A. Torabian, K. Rahimi, Performance of iron-zero (nZVI) nanno particles in removal of cephalexin from synthetic wastewater, J. Water Wastewater 25 (2014) 85–92.
[56] M.S. Legnoverde, S. Simonetti, E.I. Basaldella, Influence of pH on cephalexin adsorption onto SBA-15 mesoporous silica: Theoretical and experimental study, Appl. Surf. Sci. 300 (2014) 37–42.
[57] J. Wan, H. Deng, J. Shi, L. Zhou, T. Su, Synthesized magnetic manganese ferrite nanoparticles on activated carbon for sulfamethoxazole removal, CLEAN–Soil, Air, Water 42 (2014) 1199–1207.
[58] J. Anwar, U. Shafique, M. Salman, A. Dar, S. Anwar, Removal of Pb (II) and Cd (II) from water by adsorption on peels of banana, Bioresour. Technol. 101 (2010) 1752–1755.
[59] J.-Q. Chen, Z.-J. Hu, R. Ji, Removal of carbofuran from aqueous solution by orange peel, Desalin. Water Treat. 49 (2012) 106–114.
[60] M.J. Ahmed, S.K. Theydan, Adsorption of cephalexin onto activated carbons from Albizia lebbeck seed pods by microwave-induced KOH and K2CO3 activations, Chem. Eng. J. 211 (2012) 200–207.
[61] X. Li, J. Pan, J. Dai, X. Dai, L. Xu, X. Wei, H. Hang, C. Li, Y. Liu, Surface molecular imprinting onto magnetic yeast composites via atom transfer radical polymerization for selective recognition of cefalexin, Chem. Eng. J. 198 (2012) 503–511.
[62] M.O. Borna, M. Pirsaheb, M.V. Niri, R.K. Mashizie, B. Kakavandi, M.R. Zare, A. Asadi, Batch and column studies for the adsorption of chromium (VI) on low-cost Hibiscus Cannabinus kenaf, a green adsorbent, J. Taiwan Inst. Chem. Eng. 68 (2016) 80–89.
[63] Z. Heidarinejad, O. Rahmanian, M. Fazlzadeh, M. Heidari, Enhancement of methylene blue adsorption onto activated carbon prepared from Date Press Cake by low frequency ultrasound, J. Mol. Liq. 264 (2018) 591–599.
[64] W.J. Weber, J.C. Morris, Kinetics of adsorption on carbon from solution, J. Sanitary Eng. Div. 89 (1963) 31–60.
[65] S. Norouzi, M. Heidari, V. Alipour, O. Rahmanian, M. Fazlzadeh, F. Mohammadi-Moghadam, H. Nourmoradi, B. Goudarzi, K. Dindarloo, Preparation, characterization and Cr (VI) adsorption evaluation of NaOH-activated carbon produced from Date Press Cake; an agro-industrial waste, Bioresour. Technol. 258 (2018) 48–56.
[66] M.H. Dehghani, S. Tajik, A. Panahi, M. Khezri, A. Zarei, Z. Heidarinejad, M. Yousefi, Adsorptive removal of noxious cadmium from aqueous solutions using poly urea-formaldehyde: A novel polymer adsorbent, MethodsX 5 (2018) 1148–1155.
[67] A. Naghizadeh, H. Shahabi, F. Ghasemi, A. Zarei, Synthesis of walnut shell modified with titanium dioxide and zinc oxide nanoparticles for efficient removal of humic acid from aqueous solutions, J. Water Health 14 (2016) 989–997.
[68] M.V. Niri, A.H. Mahvi, M. Alimohammadi, M. Shirmardi, H. Golastanifar, M.J. Mohammadi, A. Naeimabadi, M. Khishdost, Removal of natural organic matter (NOM) from an aqueous solution by NaCl and surfactant-modified clinoptilolite, J. Water Health 13 (2015) 394–405.
[69] Y. Kan, Q. Yue, S. Liu, B. Gao, Effects of Cu and CuO on the preparation of activated carbon from waste circuit boards by H3PO4 activation, Chem. Eng. J. 331 (2018) 93–101.
[70] V.K. Gupta, R. Kumar, A. Nayak, T.A. Saleh, M. Barakat, Adsorptive removal of dyes from aqueous solution onto carbon nanotubes: a review, Adv. Colloid Interface Sci. 193 (2013) 24–34.
[71] G. Zhang, J. Qu, H. Liu, A.T. Cooper, R. Wu, CuFe2O4/activated carbon composite: a novel magnetic adsorbent for the removal of acid orange II and catalytic regeneration, Chemosphere 68 (2007) 1058–1066.
[72] A.A. Mohammadi, A. Zarei, H. Alidadi, M. Afsharnia, M. Shams, Two-dimensional zeolitic imidazolate framework-8 for efficient removal of phosphate from water, process modeling, optimization, kinetic, and isotherm studies, Desalination Water Treat. 129 (2018) 244–254.
[73] H. Pouretedal, N. Sadegh, Effective removal of amoxicillin, cephalexin, tetracycline and penicillin G from aqueous solutions using activated carbon nanoparticles prepared from vine wood, J. Water Process Eng. 1 (2014) 64–73.
[74] H.I. Chieng, L.B. Lim, N. Priyantha, Enhancing adsorption capacity of toxic malachite green dye through chemically modified breadnut peel: equilibrium, thermodynamics, kinetics and regeneration studies, Environ. Technol. 36 (2015) 86–97.
[75] C. Zhang, C. Lai, G. Zeng, D. Huang, C. Yang, Y. Wang, Y. Zhou, M. Cheng, Efficacy of carbonaceous nanocomposites for sorbing ionizable antibiotic sulfamethazine from aqueous solution, Water Res. 95 (2016) 103–112.

Please cite this article as: Y. Rashtbari, S. Hazrati, A. Azari et al., A novel, eco-friendly and green synthesis of PPAC-ZnO and PPAC-nZVI nanocomposite using pomegranate peel: Cephalexin adsorption experiments, mechanisms, isotherms and kinetics, Advanced Powder Technology, https://doi.org/10.1016/j.apt.2020.02.001